Pure Appl. Geophys. 171 (2014), 2111–2127

DOI 10.1007/s00024-014-0844-5

Pure and Applied Geophysics

Reflection and Transmission Coefficients for an Incident Plane Shear Wave at an Interface Separating Two Dissimilar Poroelastic Solids

Xu Liu[1] and Stewart Greenhalgh[2]

Abstract—Using Biot's poroelasticity theory, we derive expressions for the reflection and transmission coefficients for a plane shear wave incident on an interface separating two different poroelastic solids. The coefficients are formulated as a function of the wave incidence angle, frequency and rock properties. Specific cases calculated include the boundary between water-saturated sand and water-saturated sandstone and the gas–water interface in sand. The results show a very different interface response to that of an incident P wave. Plane SV wave incidence does not significantly excite the Biot slow P wave if the frequency of the wave is below the transition frequency. Above this frequency, an incident plane SV wave can generate a mode-converted slow Biot P wave which is actually a normal propagating wave and not highly attenuating as in the usual (diffusive) case. For an incident SV wave onto a gas–water interface, even at very high frequency, there is no significant Biot second P wave produced. For small incident angles, the gas–water interface is essentially transparent. With increasing angles, there can arise an unusual "definitive angle" in the reflection/transmission coefficient curves which is related to the change of fluid viscosity on both sides of the interface and provides a possible new means for underground fluid assessment.

Key words: Poroelastic media, reflection and transmission coefficients.

1. Introduction

The reflection and transmission coefficients for plane elastic waves incident on a plane boundary separating purely elastic media are well understood (Aki and Richards 1980). However, the case of two dissimilar porous media separated by a plane interface has been less well researched. The dynamic theory of wave propagation in a fluid-saturated porous solid was originally developed by Biot (1956a, b), extending the earlier static treatment of Gassmann (1951). In Biot theory, the porous rock comprises two interacting phases: the porous rock matrix and the fluid filling the interconnecting pores. The viscous fluid is allowed to flow relative to the rock skeleton, causing frictional losses or wave attenuation. Both the attenuation and the wave velocity are frequency dependent. According to the theory, two compressional waves and one rotational (shear) wave exist in such a medium. One of the compressional waves is the classic fast wave which is usually observed, whereas the other is a slow disturbance and is difficult to observe. Whilst all waves are dispersive and attenuated, the fast Biot wave exhibits very little dispersion and attenuation over several decades of frequency. By contrast, the second (slow) compressional wave propagates in the manner of a "diffusion" wave. It is highly dispersive and attenuated at low frequencies, with its phase velocity approaching zero at the zero frequency limit.

As a relatively simple and important case of reflection and transmission behaviour in porous media, Geerstma and Smit (1961) studied wave partitioning at the interface between two fluid-filled porous rocks under the special condition of normal incidence. They showed that the presence of the Biot slow P wave which is generated at the interface had an effect upon the reflection and absorption. Gurevich *et al*. (2004) derived closed-form expressions for normal-incidence reflection and transmission coefficients for an interface between fluid-saturated porous materials and showed a square root dependence on frequency. At very low frequency, it was found that the poroelastic reflection coefficient reverts to the elastic value. Dutta and Odé (1983) dealt with an obliquely incident classical P wave at a gas–water

[1] Department of Geology and Geophysics, University of Adelaide, Adelaide 5005, Australia.
[2] Institute of Geophysics, ETH Zurich, Sonneggstrasse 5, 8092 Zurich, Switzerland. E-mail: gstewart@aug.ig.erdw.ethz.ch

interface in the low frequency range. The treatment was extended into the high frequency range by SANTOS *et al*. (1992), who stressed the importance of the frequency correction. The case of oblique reflection and transmission at a fluid/porous medium interface under the rigid grain approximation and with no reflected S wave was investigated by DENNEMAN *et al*. (2002). They considered four different types of porous medium: liquid as well as air-filled clay/silt and sand. They found that in all cases over the frequency range 5–20 kHz, the fast P wave and S wave velocities in the transmitted (porous) medium were indistinguishable from the frequency-independent ones calculated using the Gassmann relations. Furthermore, they observed a striking difference in the reflection/transmission coefficients for the interface between water and an air-filled porous medium when using an open-pore or closed-pore boundary condition.

WU *et al*. (1990) and YANG (1999) studied the effect of the flow condition (interface permeability) on the reflection and transmission at an interface between two porous media. SHARMA and SAINI (1992) also considered the effect on wave reflection and transmission of pore alignment at the interface between two saturated poroelastic media. Issues related to the interface condition (hydraulic contact between the two media) were studied extensively by GUREVICH and SCHOENBERG (1999). For perfect hydraulic contact (open pores) the pressure is continuous across the interface whereas the opposite extreme of closed pores implies no motion of the fluid relative to the solid. GUREVICH and SCHOENBERG (1999) replaced the discontinuity surface by a thin transition layer in which the properties of the medium change rapidly yet continuously, and then took the limit as the thickness of the transition layer approaches zero. They found that the "open-pore" condition is the only one fully consistent with the validity of Biot's equations throughout the poroelastic continuum (including surfaces across which the medium properties are discontinuous), but their approach was also capable of handling partially blocked or completely impermeable interfaces.

Some researchers have investigated the interface behaviour for incident shear waves. The paper by WU *et al*. (1990) considered an incident shear wave in a fluid-saturated porous solid impinging on a fluid medium, whereas SHARMA *et al*. (1990) investigated P and SV waves at an interface between a linear viscoelastic solid and a liquid-saturated porous solid. However, to the best of our knowledge, no one apart from SHARMA (2008) has specifically dealt with the general problem of an incident shear wave (at arbitrary incidence angle) onto an interface between two different porous solids. SHARMA (2008) also considered the partial connection of surface pores at the porous–porous interface. Such imperfection in welded bonding is represented by tangential slipping and results in dissipation of part of the strain energy. The SHARMA (2008) study, whilst novel and insightful, considers only relatively low contrast interfaces for liquid saturated media (sandstone/limestone) and does not reveal some rather interesting peculiarities in the reflection/transmission response for other types of porous interface reported in this contribution.

The situation we numerically investigate here of unconsolidated/consolidated sediments, and changing pore fluid in a rock is of practical interest as well as being theoretically intriguing. The interface could be the boundary between two different porous rocks having the same fluid filling the pores, or it could be a gas–water interface in a porous rock. The reasons for studying the problem are varied: (1) interface responses to an incident shear wave are different to those for an incident P wave. Such knowledge could provide additional information about AVO response in seismic exploration, which until now is almost exclusively based on P waves. (2) Significant excitation of the Biot slow P wave and diffusive energy losses are known to occur at the interface between different porous rocks or at a gas–water interface for an incident P wave. However, the difference in response between the two types of interface for an incident SV wave is not well understood. It is also important to know whether the incident SV wave produces significant slow P wave excitation by mode conversion and consequent diffusive energy loss. So, a systematic investigation is needed. (3) The site responses to shear waves produced by earthquakes or other vibratory sources play a very important role in architectural design and building safety. Often, such structures are built on porous soils and rocks.

In this paper we will provide a detailed analysis of the reflection and transmission behaviour of S waves

at the interface between two different porous media. The procedure is similar to that adopted by DUTTA and ODÉ (1983) for the acoustic case.

2. Wave Equations From Biot's Theory

DUTTA and ODÉ (1979a, b; 1983) decoupled Biot's two wave equations in the low frequency range into three vector Helmholtz equations for the fluid displacement as follows:

$$(\nabla^2 + k_s^2)\mathbf{w}_s = 0 \tag{1a}$$

$$(\nabla^2 + k_d^2)\mathbf{w}_d = 0 \tag{1b}$$

$$(\nabla^2 + k_c^2)\mathbf{w}_c = 0, \tag{1c}$$

where $\mathbf{w}_\lambda(\lambda = \text{s, d, c})$ is the displacement of the fluid with respect to the solid matrix (i.e., the relative fluid displacement) or the filtration velocity which is defined as $\mathbf{w} = n(\mathbf{U} - \mathbf{u})$. Here $\mathbf{U}$ is the displacement of the fluid, $\mathbf{u}$ the displacement of the solid and n the porosity. The subscripts s, d, c denote the shear wave, diffusive (slow Biot) P wave and the classic (fast) P wave; $k_\lambda(\lambda = \text{s, d, c})$ is the wavenumber that is expressed as a function of frequency ω and the rock properties (see Appendix A for details).

For a Biot porous medium, the dispersion relations for the different wave velocities and attenuations are determined from the complex frequency-dependent wavenumbers $k_\lambda(l = \text{s, d, c}$, see Eqs. 47–49). The complex velocities $V_\lambda(\omega)$ are given by:

$$V_\lambda(\omega) = \frac{\omega}{k_\lambda(\omega)} \quad (\lambda = \text{s, d, c}) \tag{2}$$

Then the phase velocities $c_\lambda(\omega)$ and specific quality factors $Q_t(\omega)$ (attenuation $= 1/Q$) for the three waves are given by:

$$\begin{aligned} c_\lambda(\omega) &= \left(\text{Re}\left[\frac{1}{V_\lambda}\right]\right)^{-1}, \\ Q_\lambda(\omega) &= \frac{\text{Re}\left[1/V_\lambda^2\right]}{\text{Im}\left[1/V_\lambda^2\right]} \quad (\lambda = \text{s, d, c}), \end{aligned} \tag{3}$$

The linear relationships between the displacements of the solid frame $\mathbf{u}_\lambda$ and those of the fluid $\mathbf{w}_\lambda$ relative to the solid frame are:

$$\mathbf{u}_\lambda = \Gamma_\lambda \mathbf{w}_\lambda \quad (\lambda = \text{s, d, c}) \tag{4}$$

$$\Gamma_s = -\frac{q(\omega)}{\rho_f}\ \Gamma_d = \delta_c \text{ and } \Gamma_c = \delta_d \tag{5}$$

Here, ρ_f is the density of the fluid. Expressions for $q(\omega)$, δ_c and δ_d are given in Appendix A.

It should be pointed out that the Γ coefficients can have slightly different expressions, dependent on the form of the harmonic time dependence assumed. In this paper, we choose the time dependence as $\exp(-i\omega t)$, whereas DUTTA and ODÉ (1983) applied a positive exponential time dependence $\exp(i\omega t)$. In addition, the rock properties can take different notations, so we need to specify them.

The three vector Helmholtz wave equations, Eq. 1a–c, and the linear relationships, Eq. 4 provide the basis for the solution of homogeneous plane body wave propagation in porous media. By homogeneous we imply rectilinear polarization of the body waves and dissipation in the direction of propagation. By contrast, inhomogeneous waves are attenuated in a direction different to the direction of propagation and exhibit elliptical polarization. The homogeneous solution needs to satisfy an additional set of equations describing the continuity of certain physical quantities across the interface separating the two porous media. Such equations are called boundary conditions. For some simple geometric models, the wave equations can be solved analytically subject to the boundary conditions.

3. Boundary Conditions for Porous Media

Consider a surface Ω as the plane interface between the two porous media (denoted by subscripts 1 and 2), and let the unit normal vector of Ω be $\hat{\mathbf{n}}$, whose direction is assumed to be from medium 1 to medium 2. On the interface Ω, the continuity of the requisite field quantities can be written as (DERESIEWICZ and SKALAK 1963):

$$u_{1i} = u_{2i} \text{ (the frame displacement of } i \text{ th component, normal and tangential)} \tag{6}$$

$$\tau_{1ij}\hat{n}_j = \tau_{2ij}\hat{n}_j \text{ (the total traction)} \tag{7}$$

$$\hat{n}_j w_{1j} = \hat{n}_j w_{2j}$$
(the filtration velocity in the normal direction) (8)

$$\hat{n}_j \frac{\partial}{\partial t} w_{2j} = -\kappa_{12}(p_{1f} - p_{2f})$$
(the interface Darcy's law) (9a)

where κ_{12} is called the interface permeability and is a function of the porosities and pore fluid mobilities of the media. There is no theoretical or experimental work to be found in the literature describing the general interface permeability (Quiroga-Goode and Carcione 1997). But, for a sealed (closed) interface, $\kappa_{12} = 0$, which leads to:

$$\hat{n}_j w_{2j} = 0 \tag{9b}$$

and, for an open interface, $k_s = \infty$, which leads to:

$$p_{1f} = p_{2f} \quad \text{on } \Omega \tag{9c}$$

For purposes of illustration, the interface will be assumed to be an open-pore boundary condition in this paper. According to the findings of Gurevich and Schoenberg (1999), as summarized in the Introduction, this is the only condition fully consistent with the Biot equations and probably more realistic than the closed-pore condition.

4. *The Reflection and Transmission Coefficients for Shear Waves at the Interface Between Two Porous Media*

Reflection and transmission coefficients can be defined in several ways (Dutta and Odé 1983). For example, they can be defined as the ratio of the solid frame displacement amplitude for each Biot wave relative to the incident wave amplitude (S wave in this paper), or the ratio of energy fluxes. Both definitions have their own advantages and disadvantages. The definition involving displacement amplitude has a simple and explicit physical significance and is easy to measure. However, as Dutta and Odé (1983) pointed out, the shape of the amplitude curves can be very different from that of the energy curves if there is a phase difference between the conjugate field quantities (stress and displacement, or pore pressure and filtration velocity). In other words, the correctness of the coefficients using the displacement amplitude ratio is difficult to check through energy conservation. Therefore, we calculate both types of coefficients in this paper.

The incident shear wave could be either an SH wave or an SV wave. Since SH waves are independent of the P-SV waves for isotropic media and incident SH waves do not mode-convert to P or SV waves (assuming no dip perpendicular to the plane of incidence), the reflection/transmission behaviour for an incident SH wave is relatively simple to treat. For reasons of completeness the solution for this case is given in Appendix B.

The geometry for the problem under consideration is shown in Fig. 1. An incident SV wave making an arbitrary angle of incidence with the normal to the interface impinges from medium 1 onto medium 2. There are six outgoing waves: three reflections and three transmitted or refracted waves: the SV wave, the slow P wave and the classical (fast) P wave in each medium.

All waves in porous media can be represented by the relative fluid displacement. The vector potential of the relative fluid displacement of the incident SV wave $\boldsymbol{\phi}_{sv}$ can be written as:

$$\left.\begin{aligned} \boldsymbol{\phi}_{sv} &= \phi_{sv}\hat{\mathbf{z}} \\ \phi_{sv} &= A_{sv}\exp(il_{1s}y)\exp(im_{1s}x - i\omega t) \end{aligned}\right\} \tag{10}$$

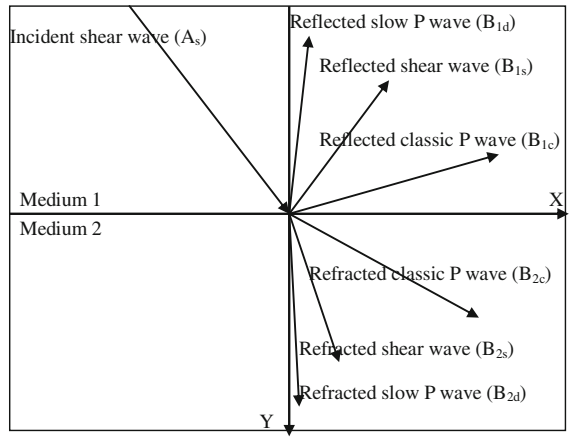

Figure 1
Reflection and refraction of an incident plane shear wave at an interface between two fluid-filled porous media. The symbols s, c and d denote, respectively, shear, classic (fast) compressional and diffusive (slow) compressional Biot waves

where $\hat{\mathbf{z}}$ is a unit vector perpendicular to the plane of incidence. Thus, the relative fluid displacement vector $\mathbf{w}_{\mathrm{sv}}$ is:

$$\mathbf{w}_{\mathrm{sv}} = \hat{\mathbf{x}}\frac{\partial}{\partial y}\phi_{\mathrm{sv}} - \hat{\mathbf{y}}\frac{\partial}{\partial x}\phi_{\mathrm{sv}} = (il_{1\mathrm{s}}\hat{\mathbf{x}} - im_{1\mathrm{s}}\hat{\mathbf{y}})\phi_{\mathrm{sv}} \quad (11)$$

The displacement potentials of the reflected waves in medium 1 include the scalar potentials ϕ_{rc} for the fast P wave and ϕ_{rd} for the slow P wave, and the vector potential $\boldsymbol{\phi}_{\mathrm{rs}}$ for the shear wave, given by:

$$\phi_{1\mathrm{c}} = B_{1\mathrm{c}}\exp(-il_{1\mathrm{c}}y)\exp(im_{1\mathrm{c}}x - i\omega t) \quad (12)$$

$$\phi_{1\mathrm{d}} = B_{1\mathrm{d}}\exp(-il_{1\mathrm{d}}y)\exp(im_{1\mathrm{d}}x - i\omega t) \quad (13)$$

$$\left.\begin{aligned}\boldsymbol{\phi}_{1\mathrm{s}} &= \phi_{1\mathrm{s}}\hat{\mathbf{z}}\\ \phi_{1\mathrm{s}} &= B_{1\mathrm{s}}\exp(-il_{1\mathrm{s}}y)\exp(im_{1\mathrm{s}}x - i\omega t)\end{aligned}\right\} \quad (14)$$

where $l_{j\lambda}$ and $m_{j\lambda}$, (λ = c, d, $s$and j = 1, 2) denote, respectively, the x- and y-components of the complex wave vector $k_{j\lambda}$ of medium j. We also have the relationship linking the components of the wave vector to the total wave vector:

$$l_{j\lambda}^2 + m_{j\lambda}^2 = k_{j\lambda}^2 \quad (15)$$

The potentials of the transmitted waves in medium 2 include $\phi_{2\mathrm{c}}$ for the fast P wave, $\phi_{2\mathrm{d}}$ for the slow P wave, and $\boldsymbol{\phi}_{2\mathrm{c}}$ for the shear wave can be written as:

$$\phi_{2\mathrm{c}} = B_{2\mathrm{c}}\exp(il_{2\mathrm{c}}y)\exp(im_{2\mathrm{c}}x - i\omega t) \quad (16)$$

$$\phi_{2\mathrm{d}} = B_{2\mathrm{d}}\exp(il_{2\mathrm{d}}y)\exp(im_{2\mathrm{d}}x - i\omega t) \quad (17)$$

$$\left.\begin{aligned}\boldsymbol{\phi}_{2\mathrm{s}} &= \phi_{2\mathrm{s}}\hat{\mathbf{z}}\\ \phi_{2\mathrm{s}} &= B_{2\mathrm{s}}\exp(il_{2\mathrm{s}}y)\exp(im_{2\mathrm{s}}x - i\omega t)\end{aligned}\right\} \quad (18)$$

From the continuity condition of the solid frame displacement, Eq. 6, and the linear relationship, Eq. 4, which are valid for all x and t on the interface $y = 0$, we have from Snell's Law:

$$m_{1\lambda} = m_{2\lambda} \quad (\lambda = \mathrm{c},\ \mathrm{d},\ \mathrm{s}) \ \text{ or} \quad (19)$$

$$k_{1s}\sin\theta_i = k_{1\lambda}\sin\theta_{1\lambda} = k_{2\lambda}\sin\theta_{2\lambda} \quad (\lambda = \mathrm{c},\ \mathrm{d},\ \mathrm{s}) \quad (20)$$

For simplicity, we set $m_{1\ \text{or}\ 2\lambda} = m$.

The relative fluid displacement vectors of the reflected waves are:

$$\mathbf{w}_{1\mathrm{c}} = \hat{\mathbf{x}}\frac{\partial}{\partial x}\phi_{1\mathrm{c}} + \hat{\mathbf{y}}\frac{\partial}{\partial y}\phi_{1\mathrm{c}} = (im\hat{\mathbf{x}} - il_{1\mathrm{c}}\hat{\mathbf{y}})\phi_{1\mathrm{c}} \quad (21)$$

$$\mathbf{w}_{1d} = \hat{\mathbf{x}}\frac{\partial}{\partial x}\phi_{1\mathrm{d}} + \hat{\mathbf{y}}\frac{\partial}{\partial y}\phi_{1\mathrm{d}} = (im\hat{\mathbf{x}} - il_{1\mathrm{d}}\hat{\mathbf{y}})\phi_{1\mathrm{d}} \quad (22)$$

$$\mathbf{w}_{1\mathrm{s}} = \hat{\mathbf{x}}\frac{\partial}{\partial y}\phi_{1\mathrm{s}} - \hat{\mathbf{y}}\frac{\partial}{\partial x}\phi_{1\mathrm{s}} = (-il_{1\mathrm{s}}\hat{\mathbf{x}} - im\hat{\mathbf{y}})\phi_{1\mathrm{s}} \quad (23)$$

The relative fluid displacement vectors of the transmitted waves are:

$$\mathbf{w}_{2\mathrm{c}} = \hat{\mathbf{x}}\frac{\partial}{\partial x}\phi_{2\mathrm{c}} + \hat{\mathbf{y}}\frac{\partial}{\partial y}\phi_{2\mathrm{c}} = (im\hat{\mathbf{x}} + il_{2\mathrm{c}}\hat{\mathbf{y}})\phi_{2\mathrm{c}} \quad (24)$$

$$\mathbf{w}_{2\mathrm{d}} = \hat{\mathbf{x}}\frac{\partial}{\partial x}\phi_{2\mathrm{d}} + \hat{\mathbf{y}}\frac{\partial}{\partial y}\phi_{2\mathrm{d}} = (im\hat{\mathbf{x}} + il_{2\mathrm{d}}\hat{\mathbf{y}})\phi_{2\mathrm{d}} \quad (25)$$

$$\mathbf{w}_{2\mathrm{s}} = \hat{\mathbf{x}}\frac{\partial}{\partial y}\phi_{2\mathrm{s}} - \hat{\mathbf{y}}\frac{\partial}{\partial x}\phi_{2\mathrm{s}} = (il_{2\mathrm{s}}\hat{\mathbf{x}} - im\hat{\mathbf{y}})\phi_{2\mathrm{s}} \quad (26)$$

In medium 1, the relative fluid displacement vector $\mathbf{w}_1$, and the displacement vector of the solid frame $\mathbf{u}_1$ can be written as:

$$\mathbf{w}_1 = \mathbf{w}_{\mathrm{sv}} + \mathbf{w}_{1\mathrm{s}} + \mathbf{w}_{1\mathrm{c}} + \mathbf{w}_{1\mathrm{d}} \quad (27)$$

$$\mathbf{u}_1 = \Gamma_{1\mathrm{s}}(\mathbf{w}_{\mathrm{sv}} + \mathbf{w}_{1\mathrm{s}}) + \Gamma_{1\mathrm{c}}\mathbf{w}_{1\mathrm{c}} + \Gamma_{1\mathrm{d}}\mathbf{w}_{1\mathrm{d}} \quad (28)$$

In medium 2, the displacement vector of the relative fluid motion $\mathbf{w}_2$, and that of the solid frame $\mathbf{u}_2$ can be written as:

$$\mathbf{w}_2 = \mathbf{w}_{2\mathrm{s}} + \mathbf{w}_{2\mathrm{c}} + \mathbf{w}_{2\mathrm{d}} \quad (29)$$

$$\mathbf{u}_2 = \Gamma_{2\mathrm{s}}\mathbf{w}_{2\mathrm{s}} + \Gamma_{2\mathrm{c}}\mathbf{w}_{2\mathrm{c}} + \Gamma_{2\mathrm{d}}\mathbf{w}_{2\mathrm{d}} \quad (30)$$

The coefficient A_{sv} in Eq. 10 is assumed to be known, and the six coefficients $B_{j\lambda}$ (j = 1, 2; λ = s, c, d) in Eqs. 12–14 and 16–18 are unknown and must be determined from the six boundary conditions.

By the boundary conditions and Biot's stress–strain relations (Eqs. 59 and 60), on the interface $y = 0$, we obtain the matrix equation:

$$\mathbf{AB} = \mathbf{C} \quad (31)$$

The elements of $\mathbf{A}$ are $a_{ij}(i, j = 1, 2,\ldots 6)$ which are written out explicitly in Appendix C; the vectors C and B are given by:

$$\mathbf{C} = [1 \quad 1 \quad 1 \quad 1 \quad 1 \quad 0]^{\mathrm{T}} \quad (32)$$

$$\mathbf{B} = [B_{1\mathrm{s}} \quad B_{1\mathrm{c}} \quad B_{1\mathrm{d}} \quad B_{2\mathrm{s}} \quad B_{2\mathrm{c}} \quad B_{2\mathrm{d}}]^{\mathrm{T}}\big/A_{\mathrm{sv}} \quad (33)$$

The first three elements of B are the reflections and the last three elements are transmissions of the relative fluid displacement potentials.

The reflection $R_\lambda(\lambda = \mathrm{s, c, d})$ and transmission $T_\lambda(\lambda = \mathrm{s, c, d})$ coefficients are referred to as amplitude ratios and are defined as the complex ratios of the solid frame displacement amplitude of the appropriate Biot wave to that of the incident wave amplitude (here taken to be an SV wave). By this definition (Dutta and Odé 1983), we get similar coefficient equations including the absolute values of the complex ratios and their arguments for SV-incidence. However, we judge that the phase differences between the scattered waves and the incident wave are more instructive than the arguments. This makes our equations slightly different from those of Dutta and Odé (1983), despite the different type of incident wave as well.

To illustrate this, the solid frame displacements can be expressed in the following way:

The solid frame displacement of the incident SV wave is:

$$\mathbf{u}_{\mathrm{sv}} = \Gamma_{1\mathrm{s}}(il_{1\mathrm{s}}\hat{\mathbf{x}} - im\hat{\mathbf{y}})A_{\mathrm{sv}}\exp(il_{1\mathrm{s}}y)\exp(imx - i\omega t) \tag{34}$$

The solid frame displacements of the reflected waves are:

$$\left.\begin{aligned}\mathbf{u}_{1\mathrm{s}} &= \Gamma_{1\mathrm{s}}(-il_{1\mathrm{s}}\hat{\mathbf{x}} - im\hat{\mathbf{y}})B_{1\mathrm{s}}\exp(-il_{1\mathrm{s}}y)\exp(imx - i\omega t)\\ \mathbf{u}_{1\mathrm{c}} &= \Gamma_{1\mathrm{c}}(im\hat{\mathbf{x}} - il_{1\mathrm{c}}\hat{\mathbf{y}})B_{1\mathrm{c}}\exp(-il_{1\mathrm{c}}y)\exp(imx - i\omega t)\\ \mathbf{u}_{1\mathrm{d}} &= \Gamma_{1\mathrm{d}}(im\hat{\mathbf{x}} - il_{1\mathrm{d}}\hat{\mathbf{y}})B_{1\mathrm{d}}\exp(-il_{1\mathrm{d}}y)\exp(imx - i\omega t)\end{aligned}\right\} \tag{35}$$

The solid frame displacements of the transmitted (refracted) waves are:

$$\left.\begin{aligned}\mathbf{u}_{2\mathrm{s}} &= \Gamma_{2\mathrm{s}}(il_{2\mathrm{s}}\hat{\mathbf{x}} - im\hat{\mathbf{y}})B_{2\mathrm{s}}\exp(il_{2\mathrm{s}}y)\exp(imx - i\omega t)\\ \mathbf{u}_{2\mathrm{c}} &= \Gamma_{2\mathrm{c}}(im\hat{\mathbf{x}} - il_{2\mathrm{c}}\hat{\mathbf{y}})B_{2\mathrm{c}}\exp(il_{2\mathrm{c}}y)\exp(imx - i\omega t)\\ \mathbf{u}_{2\mathrm{d}} &= \Gamma_{2\mathrm{d}}(im\hat{\mathbf{x}} - il_{2\mathrm{d}}\hat{\mathbf{y}})B_{2\mathrm{d}}\exp(il_{2\mathrm{d}}y)\exp(imx - i\omega t)\end{aligned}\right\} \tag{36}$$

It is easy to see that the negative signs in the three reflected waves imply a 180° phase difference with respect to the incident wave (which is travelling in the opposite y direction), even at the coordinate origin. They should be compensated. Therefore, we have:

$$\left.\begin{aligned}R_{\mathrm{s}}\exp(i[\theta_{\mathrm{s}} + 180^\circ]) &= \frac{B_{1\mathrm{s}}}{A_{\mathrm{sv}}}, \quad R_{\mathrm{c}}\exp(i[\theta_{\mathrm{c}} + 180^\circ]) = \frac{B_{1\mathrm{c}}\Gamma_{1\mathrm{c}}k_{1\mathrm{c}}}{A_{\mathrm{sv}}\Gamma_{1\mathrm{s}}k_{1\mathrm{s}}},\\ R_{\mathrm{d}}\exp(i[\theta_{\mathrm{d}} + 180^\circ]) &= \frac{B_{1\mathrm{d}}\Gamma_{1\mathrm{d}}k_{1\mathrm{d}}}{A_{\mathrm{sv}}\Gamma_{1\mathrm{s}}k_{1\mathrm{s}}}, \quad T_{\mathrm{s}}\exp(i\varphi_{\mathrm{s}}) = \frac{B_{2\mathrm{s}}\Gamma_{2\mathrm{s}}k_{2\mathrm{s}}}{A_{\mathrm{sv}}\Gamma_{1\mathrm{s}}k_{1\mathrm{s}}},\\ T_{\mathrm{c}}\exp(i\varphi_{\mathrm{c}}) &= \frac{B_{2\mathrm{c}}\Gamma_{2\mathrm{c}}k_{2\mathrm{c}}}{A_{\mathrm{sv}}\Gamma_{1\mathrm{s}}k_{1\mathrm{s}}}, \quad T_{\mathrm{d}}\exp(\mathrm{i}\varphi_{\mathrm{d}}) = \frac{B_{2\mathrm{d}}\Gamma_{2\mathrm{d}}k_{2\mathrm{d}}}{A_{\mathrm{sv}}\Gamma_{1\mathrm{s}}k_{1\mathrm{s}}}\end{aligned}\right\} \tag{37}$$

Here, θ_λ and φ_λ ($\lambda = \mathrm{s, c, d}$) represent the phase differences between the reflected and transmitted waves, relative to the incident wave. They are slightly different from the arguments of the amplitude reflection and transmission coefficients applied in other papers (for example, Dutta and Odé 1983; Sharma *et al.* 1990).

Although our time dependence and the rock properties are different from those of Dutta and Odé (1983), the derivation about energy flux in what follows is very similar. Energy flux in their paper can be defined as the rate at which work is done by the appropriate wave per unit area across the interface (take $y = 0$) and it can be written as:

$$F_{i\cdot\lambda} = \frac{\omega}{2\pi}\int_0^{2\pi/\omega}\left[(\tau_{yy})_i(\dot{u}_y)_\lambda + (\tau_{xy})_i(\dot{u}_x)_\lambda - (p)_i(\dot{w}_y)_\lambda\right]\mathrm{d}t \tag{38}$$

Here, τ and p are the total stress tensor and the pore pressure (Eqs. 59 and 60) in medium i; the subscript λ carries the notation of the appropriate wave. Because there are several types of waves in each medium on either side of the interface, the total energy flux is composed of the orthodox fluxes and the interference fluxes. The orthodox fluxes comprise the stresses and incremental displacements pertaining to the same Biot wave type, whereas the interference fluxes comprise the stresses and incremental displacements pertaining to different Biot waves (mixed terms). The interference fluxes arise as a result of the inhomogeneous nature of the wave (i.e., absorbing Biot media), but vanish in the classical perfectly elastic medium case (homogeneous waves). The interference fluxes also go to zero at normal incidence. They are generally small at seismic frequencies but become important at ultrasonic frequencies encountered in sonic logging (see Dutta and Odé 1983). The conservation of the total energy across the interface can be written as:

$$\left.\begin{aligned} F_{\mathrm{I}} = &-F_{1\mathrm{s}.1\mathrm{s}} - F_{1\mathrm{c}.1\mathrm{c}} - F_{1\mathrm{d}.1\mathrm{d}} + F_{2\mathrm{s}.2\mathrm{s}} + F_{2\mathrm{c}.2\mathrm{c}} + F_{2\mathrm{d}.2\mathrm{d}} \\ &-F_{1\mathrm{s}.1\mathrm{c}} - F_{1\mathrm{c}.1\mathrm{d}} - F_{1\mathrm{d}.1\mathrm{s}} + F_{2\mathrm{s}.2\mathrm{c}} + F_{2\mathrm{c}.2\mathrm{d}} + F_{2\mathrm{d}.2\mathrm{s}} \end{aligned}\right\} \tag{39}$$

where F_{I} is incident energy flux and is given by:

$$F_{\mathrm{I}} = F_{i.i} + F_{i.1\mathrm{s}} + F_{i.1\mathrm{c}} + F_{i.1\mathrm{d}} \tag{40}$$

In the above equations, both parts of the subscript which are separated by the symbol '.' denote the notation of the waves. The orthodox fluxes refer to the items with repeated subscripts and the interference fluxes refer to the other terms in which the two subscripts are dissimilar. Completing the integral leads to equations for the energy fluxes. For example, for the orthodox flux $F_{1\mathrm{s}.1\mathrm{s}}$, we have:

$$\left.\begin{aligned} F_{1\mathrm{s}.1\mathrm{s}} = &\frac{\omega\pi}{2}\left[\mathrm{Re}(\tau_{yy})_{1\mathrm{s}}\mathrm{Im}(u_y)_{1\mathrm{s}} - \mathrm{Im}(\tau_{yy})_{1\mathrm{s}}\mathrm{Re}(u_y)_{1\mathrm{s}}\right] \\ &+\frac{\omega\pi}{2}\left[\mathrm{Re}(\tau_{xy})_{1\mathrm{s}}\mathrm{Im}(u_x)_{1\mathrm{s}} - \mathrm{Im}(\tau_{xy})_{1\mathrm{s}}\mathrm{Re}(u_x)_{1\mathrm{s}}\right] \\ &-\frac{\omega\pi}{2}\left[\mathrm{Re}(p)_{1\mathrm{s}}\mathrm{Im}(w_y)_{1\mathrm{s}} - \mathrm{Im}(p)_{1\mathrm{s}}\mathrm{Re}(w_y)_{1\mathrm{s}}\right] \end{aligned}\right\} \tag{41}$$

and for the interference flux $F_{1\mathrm{s}.1\mathrm{c}}$, we have:

$$\left.\begin{aligned} F_{1\mathrm{s}.1\mathrm{c}} = &\frac{\omega\pi}{2}\left[\mathrm{Re}(\tau_{yy})_{1\mathrm{s}}\mathrm{Im}(u_y)_{1\mathrm{c}} - \mathrm{Im}(\tau_{yy})_{1\mathrm{s}}\mathrm{Re}(u_y)_{1\mathrm{c}}\right] \\ &+\frac{\omega\pi}{2}\left[\mathrm{Re}(\tau_{yy})_{1\mathrm{c}}\mathrm{Im}(u_y)_{1\mathrm{s}} - \mathrm{Im}(\tau_{yy})_{1\mathrm{c}}\mathrm{Re}(u_y)_{1\mathrm{s}}\right] \\ &+\frac{\omega\pi}{2}\left[\mathrm{Re}(\tau_{xy})_{1\mathrm{s}}\mathrm{Im}(u_x)_{1\mathrm{c}} - \mathrm{Im}(\tau_{xy})_{1\mathrm{s}}\mathrm{Re}(u_x)_{1\mathrm{c}}\right] \\ &+\frac{\omega\pi}{2}\left[\mathrm{Re}(\tau_{xy})_{1\mathrm{c}}\mathrm{Im}(u_x)_{1\mathrm{s}} - \mathrm{Im}(\tau_{xy})_{1\mathrm{c}}\mathrm{Re}(u_x)_{1\mathrm{s}}\right] \\ &-\frac{\omega\pi}{2}\left[\mathrm{Re}(p)_{1\mathrm{s}}\mathrm{Im}(w_y)_{1\mathrm{c}} - \mathrm{Im}(p)_{1\mathrm{s}}\mathrm{Re}(w_y)_{1\mathrm{c}}\right] \\ &-\frac{\omega\pi}{2}\left[\mathrm{Re}(p)_{1\mathrm{c}}\mathrm{Im}(w_y)_{1\mathrm{s}} - \mathrm{Im}(p)_{1\mathrm{c}}\mathrm{Re}(w_y)_{1\mathrm{s}}\right] \end{aligned}\right\} \tag{42}$$

Then, the energy reflection coefficients RE_λ (λ = s, c, d) and the energy transmission coefficients TE_λ(λ = s, c, d) are called energy ratios and are defined by the ratio of the orthodox flux and F_{I} as follows:

$$\left.\begin{aligned} \mathrm{RE_s} = \frac{F_{1\mathrm{s}.1\mathrm{s}}}{F_{\mathrm{I}}}, \quad \mathrm{RE_c} = \frac{F_{1\mathrm{c}.1\mathrm{c}}}{F_{\mathrm{I}}}, \quad \mathrm{RE_d} = \frac{F_{1\mathrm{d}.1\mathrm{d}}}{F_{\mathrm{I}}} \\ \mathrm{TE_s} = \frac{F_{2\mathrm{s}.2\mathrm{s}}}{F_{\mathrm{I}}}, \quad \mathrm{TE_c} = \frac{F_{2\mathrm{c}.2\mathrm{c}}}{F_{\mathrm{I}}}, \quad \mathrm{TE_d} = \frac{F_{2\mathrm{d}.2\mathrm{d}}}{F_{\mathrm{I}}} \end{aligned}\right\} \tag{43}$$

The interference energy fluxes are not explicitly included in the coefficients, although they appear indirectly through the denominator term. These interference fluxes are also very important for checking energy conservation. Unless proper care is taken of the interference fluxes, the energy fluxes (i.e., orthodox only) across the interface cannot be balanced. Dividing both sides of Eq. 39 by F_{I} leads to:

$$1 = \mathrm{OER} + \mathrm{IER} \tag{44}$$

Here

$$\mathrm{OER} = (-F_{1\mathrm{s}.1\mathrm{s}} - F_{1\mathrm{c}.1\mathrm{c}} - F_{1\mathrm{d}.1\mathrm{d}} + F_{2\mathrm{s}.2\mathrm{s}} + F_{2\mathrm{c}.2\mathrm{c}} + F_{2\mathrm{d}.2\mathrm{d}})/F_{\mathrm{I}} \tag{45}$$

$$\mathrm{IER} = (-F_{1\mathrm{s}.1\mathrm{c}} - F_{1\mathrm{c}.1\mathrm{d}} - F_{1\mathrm{d}.1\mathrm{s}} + F_{2\mathrm{s}.2\mathrm{c}} + F_{2\mathrm{c}.2\mathrm{d}} + F_{2\mathrm{d}.2\mathrm{s}})/F_{\mathrm{I}} \tag{46}$$

OER is called the orthodox energy ratio and IER is the interference energy ratio. We will show in the following numerical examples that IER can have a significant influence in the case of an incident SV wave. This is quite different from other published results. The loss of seismic energy from the incident wave is mainly due to the mode-converted slow Biot wave at the interface, which propagates away from the boundary in the manner of a diffusive process. At low frequency, it has largely died out within a distance of a few wavelengths.

To acquire physical insight on the wave partitioning at the poroelastic boundary it would be necessary to derive closed form expressions for the reflection and transmission coefficients. Unfortunately, the expressions are extremely complicated even for the normal-incidence case and so this is not entirely possible. All that one can do is present numerical solutions and offer some commentary on the salient features.

5. Numerical Examples of SV Wave Incidence

In this section, the formulas derived in the previous section will be applied to calculate the reflection and transmission coefficients for a variety of wave incidence angles and frequencies. The two porous media chosen are fluid-saturated sand and fluid-saturated sandstone. The two fluids are water (with subscript w) and air or gas (with subscript g).

Table 1

Material properties of the sample rocks and fluids

Parameter	Sandstone	Sand	Parameter	Water	Gas
K_s (N m^{-2})	3.9e+10	3.9e+10	K_f (N m^{-2})	2.3e+9	2.2e+7
ρ_s (kg m^{-3})	2,650	2,650	ρ_f (kg m^{-3})	1,000	100
K_m (N m^{-2})	2.23e+10	6.85e+8	η_f (kg m^{-1} s^{-1})	0.001	1.5e−5
μ (N m^{-2})	2.20e+10	4.11e+8	*Dynamic permeability relationship*		
κ_0 (m^2)	1.0e−14	1.0e−10	$T = n^{-1}$	Tortuosity	
n	0.2	0.3	$\Lambda = \sqrt{8K_0T/n}$	Pore volume-to-surface ratio	

The material properties (taken from Dutta and Odé 1983) are given in Table 1. The physical meaning of the various parameters appearing in Table 1 is explained in Appendix A.

From Eq. 58, the transition frequencies f_t of the water-saturated sandstone, water-saturated sand and gas-saturated sand are 640 kHz, 143 Hz and 21.5 Hz, respectively. By Eq. 3, we get the dispersive phase velocities c and attenuation values $1/Q$ for the above sample rocks at frequencies of 10 Hz and 100 kHz respectively which are chosen for the numerical calculation. They are listed in Table 2.

Table 2

Dispersion values for the sample rocks and fluids

Rocks	f_t (Hz)	f (Hz)	c_s (m/s)	c_c (m/s)	c_d (m/s)	$1/Q$
Water-filled sandstone	6.4e+5	10	3,079	4,807	3.6	51,183
		1.0e+5	3,080	4,808	328	5.1
Water-filled sand	143	10	437	1,897	111	12
		1.0e+5	446	1,927	309	0.02
Gas-filled sand	21.5	10	467	832	183	1.7
		1.0e+5	468	832	249	0.01

5.1. SV Wave Incident from Sandstone onto Sand

Here we consider the situation of an incident SV wave in water-saturated sandstone impinging on an interface separating such a medium from water-saturated sand. Since sand normally overlies sandstone, this would normally correspond in geology to a wave incident from below on its passage to the surface of the earth. Note that since the S wave velocity in the incident medium is greater than the P wave velocity in the transmitted medium no critical refraction is possible. We first set the incident wave frequency to 10 Hz, which is much below the transition frequency of either medium. Figure 2 shows the amplitude ratio plotted as a function of the incidence angle. The corresponding phase difference curve is shown in Fig. 3. Note that an increase in the amplitude ratio for reflected waves is not necessarily accompanied by a decrease in the corresponding amplitude ratio for the transmitted wave because of the dissipative nature of poroelastic media. The bulk and relative fluid displacements are out of phase with the bulk stress and the fluid pressure. A rise in the reflection or transmission coefficient does not necessarily mean an accompanying rise in the corresponding energy ratio.

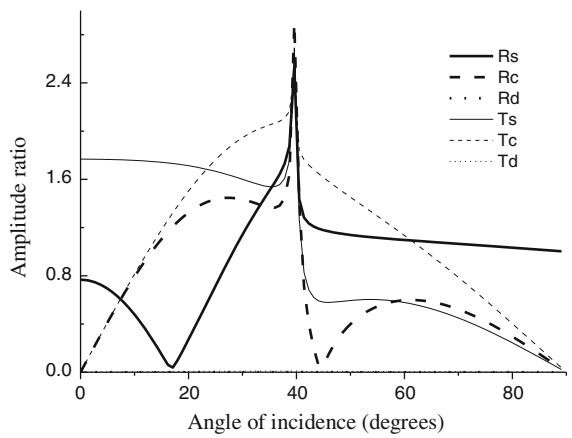

Figure 2
Incidence angle dependence of the reflected and transmitted amplitude ratios for an incident SV wave of 10 Hz frequency in water-saturated sandstone impinging on an interface with water-saturated sand. In this and subsequent amplitude ratio figures, the *symbols* denoting the different curves are defined as follows. R_s reflected shear wave, R_c reflected fast compressional wave, R_d reflected slow compressional wave, T_s transmitted shear wave, T_c transmitted fast Biot wave, T_d transmitted slow Biot wave

As expected, the Biot diffusive wave (slow P) almost does not exist (is very small) on both sides of

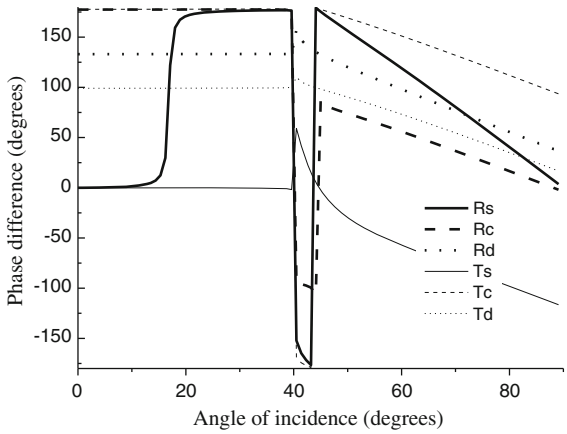

Figure 3
Incidence angle dependence of the phase differences for the reflected and transmitted waves for an SV wave of 10 Hz frequency in water-saturated sandstone impinging onto water-saturated sand

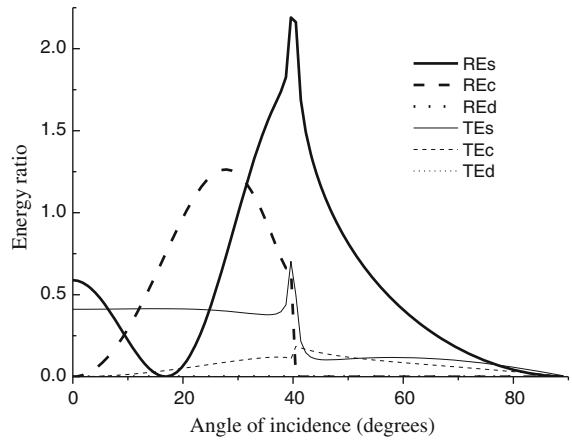

Figure 4
Energy ratios for reflected and transmitted waves for an incident plane SV wave of 10 Hz frequency in water-saturated sandstone impinging on an interface with water-saturated sand. The symbols identifying each curve for the various waves are as defined in Fig. 2, but the additional "E" now stands for energy ratio

the interface. It is very hard to even see it on plots of Fig. 2 because of the scale used to display the other waves. The amplitude ratios for the reflected S wave (R_s) and the reflected fast compressional wave (R_c) achieve maximal values at an incidence angle of $\sim 40°$ which is close to the Snell critical angle ($\sin^{-1}(3{,}079/4{,}807) = 39.8°$) for the mode-converted P wave reflected at an angle of 90° (i.e., parallel to the interface). The amplitude ratio curve for the reflected P wave also exhibits local maxima at angles of $\sim 28°$ and $\sim 60°$. With increasing incidence angle the amplitude ratio of the reflected SV wave, R_s, gradually approaches 1. The reflected waves R_s and R_c have a similar pattern of amplitude ratio and phase difference to those for an SV wave in pure elastic media and reflected at a free surface (see AKI and RICHARDS 1980). Note that a phase difference of $-180°$ is the same as that of 180°, since the entire period is 360°. The result can be appreciated by realizing that our sample sand is much softer than the sandstone (see Table 2) from which the SV wave is incident.

The energy ratios are shown in Fig. 4. They display very different patterns to the amplitude ratios given in Fig. 2. It is very interesting to observe that the energy ratio RE_c of the reflected fast P wave achieves its maximum value at an incidence angle of $\sim 28°$ whereas the reflected SV wave has its maximum at $\sim 40°$. At angles larger than these, the energy ratios RE_c and RE_s tend to zero. The Biot slow wave coefficients RE_d and TE_d achieve their maximum values of 0.1 and 0.05 %, respectively, at the critical angle. As shown in Fig. 4, the energy ratios can be larger than 1. This does not mean our results violate energy conservation (Eq. 44), which is well satisfied and shown in Fig. 5. It is only the sum of the orthodox energy flux ratio and the interference energy flux ratio for all waves which must total unity. At normal incidence there is no interference energy flux and so the energy ratios in Fig. 4 do indeed sum to 1.

We now change the wave frequency to 100 kHz, which is much higher than the transition frequency of sand, but lower than that of sandstone (see Table 2). At this frequency, the Biot slow P wave in sand changes from being diffusive to a propagating wave with a low attenuation factor ($1/Q$) of 0.02 and a phase velocity of 309 m/s. But the Biot slow P wave in sandstone is still diffusive and highly attenuating. The amplitude ratios and the energy ratios are shown in Figs. 6 and 7, respectively. They have a similar pattern to those for the 10 Hz case, plotted in Figs. 2 and 4. Figure 6 shows small but still significant values for the transmitted slow P wave amplitude ratio (c.f. Fig. 2 where it is extremely small), while Fig. 7 shows its distinct negative energy ratio. The latter means that the energy flux vector is in the reverse direction to the incident energy flux vector.

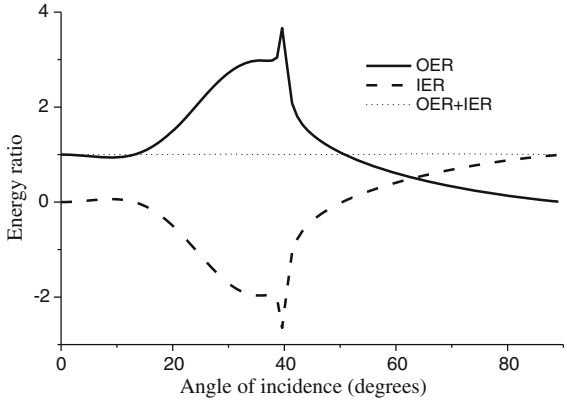

Figure 5
Orthodox energy flux and interference energy flux versus incidence angle for a plane SV wave of 10 Hz frequency in water-saturated sandstone impinging onto water-saturated sand. Note that either quantity alone can exceed 1, but their sum cannot (energy conservation)

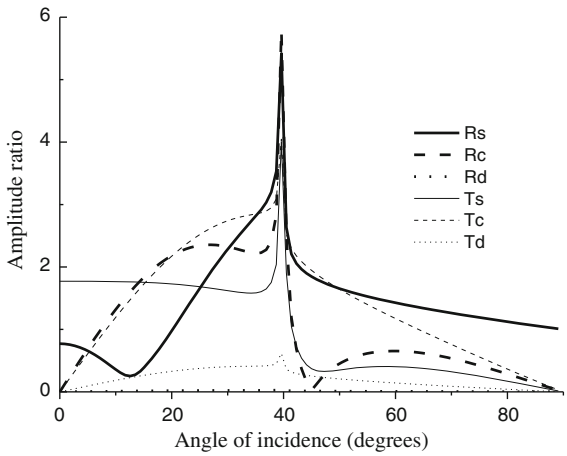

Figure 6
Incidence angle dependence of the amplitude ratios for an SV wave of frequency 100 kHz in water-saturated sandstone impinging on an interface with water-saturated sand

The phase difference and energy conservation have been calculated (not shown) and exhibit similar trends to the 10 Hz incidence wave case. Note once again that at 0° (normal incidence) the energy ratios plotted in Fig. 7 sum to unity.

5.2. SV Wave from Sand onto Sandstone

Next we consider the reverse situation of an incident SV wave in the water-saturated sand impinging on an interface separating it from water-saturated sandstone. This would correspond to the more usual case under consideration of a wave incident from above. The S wave velocity in the transmitted medium is now greater than that in the incident medium so critical refraction can occur for both the transmitted SV wave and the transmitted fast P wave. The incident wave frequency is 10 Hz. The variation of reflection and transmission coefficients is mainly over the incidence angle range from 0 to 20°. The amplitude ratio dependence on the incident angle is shown in Fig. 8 over the range 0–30°. The Biot slow P wave is again very small on both sides of the interface. The peak in R_c (and the corresponding trough in R_s) at around 5° corresponds to the critical angle [$\sin^{-1}(437/4{,}807) = 5.2°$] for the transmitted P wave at which T_s and T_c achieve their maxima. The minimum in amplitude for the reflected S wave (R_s) at an incidence angle of around 13° corresponds to the critical angle [$\sin^{-1}(437/1{,}897) = 13.3°$] at which the reflected P emerges at 90° (parallel to the boundary). At this incidence angle the reflected P wave achieves its maximum amplitude. Beyond this angle the reflected P as well as the transmitted SV and P waves become inhomogeneous (evanescent) waves with amplitudes tending towards zero, whereas the amplitude ratio of the reflected SV wave (R_s) plateaus at 1.

The energy ratios are shown in Fig. 9. They display a different pattern to the amplitude ratios in

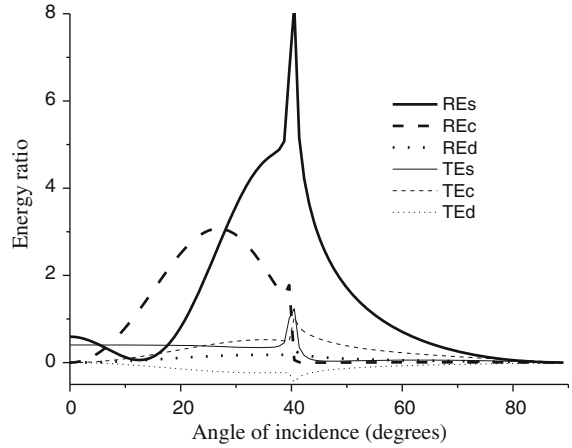

Figure 7
Energy ratios for reflected and transmitted waves for an incident plane SV wave of frequency 100 kHz in water-saturated sandstone impinging on an interface with water-saturated sand

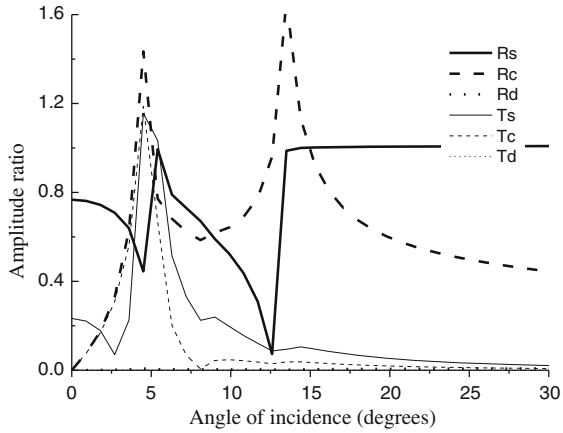

Figure 8
Incidence angle dependence of the reflected and transmitted amplitude ratios for an incident SV wave of frequency 10 Hz in water-saturated sand impinging on an interface with water-saturated sandstone. This is the reverse of the situation depicted in Fig. 2

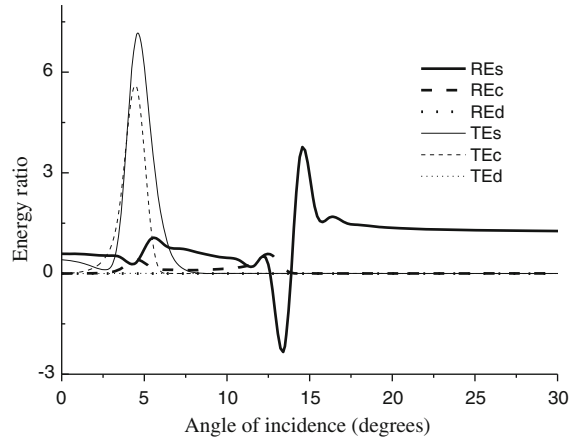

Figure 9
Incidence angle dependence of the energy ratios for a plane SV wave of frequency 10 Hz in water-saturated sand impinging onto an interface with water-saturated sandstone

Fig. 8. The Biot slow wave energy ratios RE_d and TE_d achieve their maxima of about 1 %, although they are not clearly visible in Fig. 9. It is very interesting to observe that the energy ratio REs of the reflected SV wave shows a negative value near its critical incidence angle. Energy conservation has been checked and is shown in Fig. 10 over the incidence angle range from 0 to 90°.

5.3. *SV Wave from Gas-Saturated Sand onto Water-Saturated Sand*

Here we consider the case of an incident SV wave in gas-filled sand impinging on a water-filled sand layer. There is no critical refraction of the SV wave because the S wave velocity in the transmitted medium is slightly less than that in the incident medium. However, there is a substantial velocity increase for the transmitted P wave, and so critical refraction of this mode converted wave is possible. The wave frequency is 10 Hz, which is below the transition frequencies for both the gas sand and the water-saturated sands. Figures 11 and 12 show the amplitude and energy ratios, respectively, plotted as a function of incidence angle. The Biot slow P wave is very small on both sides of the interface, and its energy ratios RE_d and TE_d are both <0.2 %. From Table 2, we see that the Snell critical angle for the

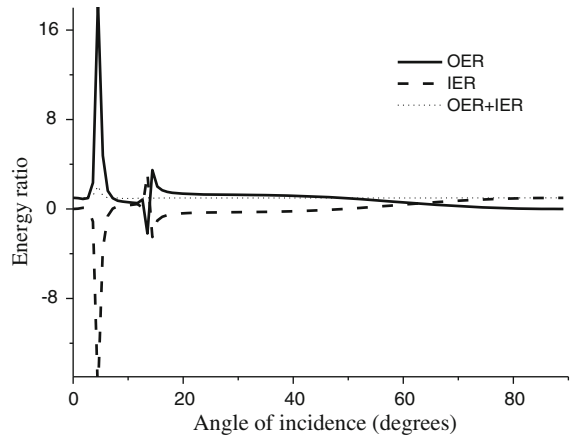

Figure 10
Orthodox energy flux and interference energy flux versus incidence angle for a plane SV wave of frequency 10 Hz in water-saturated sand impinging on an interface with water-saturated sandstone

transmitted P wave is 14.2° ($\sin^{-1}$[467/1,897]). At this angle the amplitude ratios of the transmitted P and transmitted SV waves reach their maximum values.

The Snell critical angle of incidence for the reflected P wave (reflection angle 90°) is $\sin^{-1}$(467/832) or 34°, beyond which the transmitted S wave amplitude ratio abruptly decreases. At an incidence angle of 44°, the two reflected waves, fast P and S, achieve their maximum values, while the transmitted S wave reaches its minimum; it seems to be a type of critical angle in that it represents a sudden change in

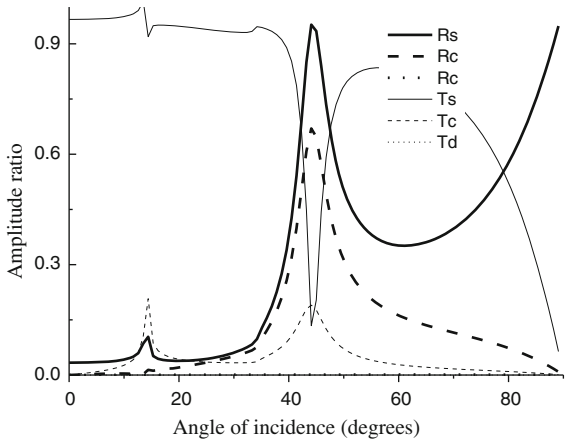

Figure 11
Incidence angle dependence of the amplitude ratios for an SV wave of frequency 10 Hz in gas-saturated sand impinging on an interface with water-saturated sand

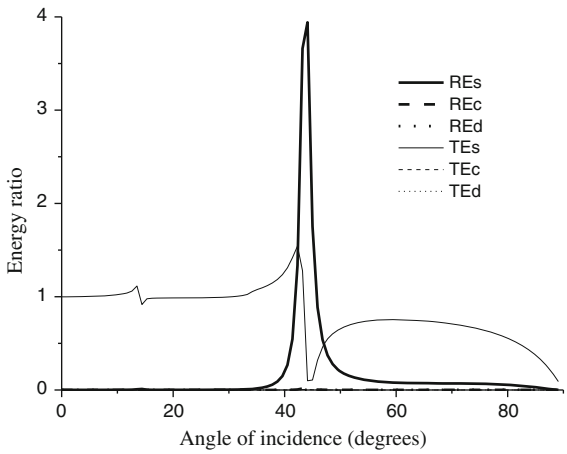

Figure 12
Incidence angle dependence of the energy ratios for a plane SV wave of frequency 10 Hz in gas-saturated sand impinging on an interface with water-saturated sand

the plot. However we don't expect a critical angle (in the usual sense of the word) at this value according to Snell's law. So, we call it an unusual definitive (diagnostic) angle. This phenomenon also occurs in the energy ratio curves (see Fig. 12). From Fig. 12, it is clear that if the incidence angle is below the critical angle of the reflected P wave, the energy ratio and the amplitude ratio of the transmitted SV wave are almost 1, which implies the gas–water interface is transparent for small incidence angles. This is even further accentuated for a wave frequency of 100 kHz, which is well beyond the transition frequencies for

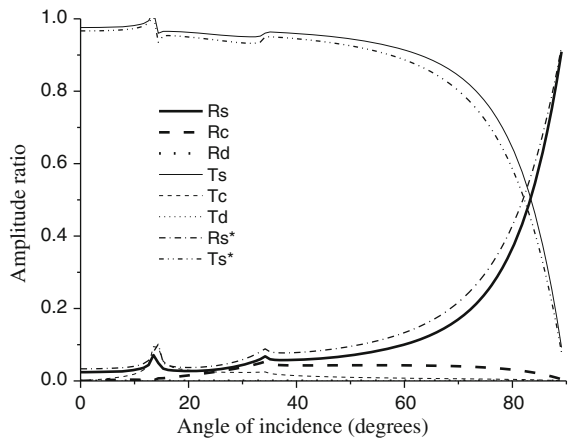

Figure 13
Incidence angle dependence of the amplitude ratios for an SV wave of frequency 100 kHz in gas-saturated sand impinging on an interface with water-saturated sand. *Symbols* R_s^* and T_s^* denote the amplitude ratios for the gas having the same viscosity as the water and an incident wave frequency of 10 Hz

media on both sides of the interface (see Figs. 13 and 14). The energy conservation law is clearly validated in Fig. 15. Here we observe that the interference energy fluxes are negligible at near-normal incidence and become negative with increasing angle, before rising sharply to equal the orthodox fluxes of +0.5 at an incidence angle of 90°.

The corresponding case of an incident fast P wave at a gas–water interface has been studied by Dutta and Odé (1983). Their Fig. 9 shows the angle-dependent reflection and transmission coefficients for the compressional wave at frequencies of 100 Hz and 10 kHz. In common with the incident S wave case investigated here, a peak is found in both curves at an angle of around 43° in the 100 Hz case; the transmitted wave is substantially larger than the reflected wave. At higher frequency (10 kHz), the peak changes to a sudden upward flexure in both coefficient curves, which are somewhat smaller (<10 %) than in the 100 Hz case. They attribute the higher frequency behavior to the fluid flow effect, which reduces the acoustic impedance contrast between the two media substantially, thus decreasing R_c and T_c. Dutta and Odé (1983) observed an energy loss due to the slow Biot wave generated at the boundary of approximately 1.7 % at 100 Hz for P waves at normal-incidence, rising to a maximum of 5.5 % at the critical angle (43°). The

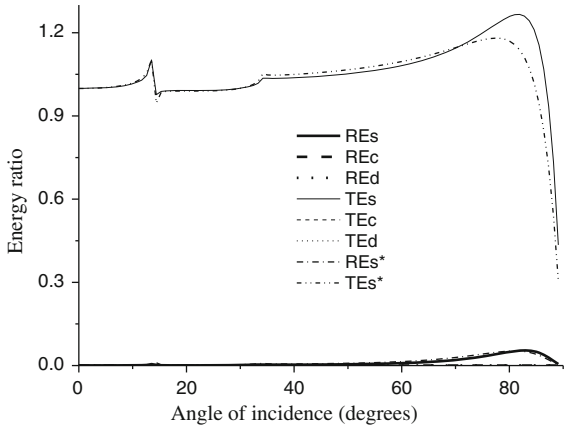

Figure 14
Incidence angle dependence of the energy ratios for an SV wave of frequency 100 kHz in gas-saturated sand impinging on an interface with water-saturated sand. *Symbols* R_s^* and T_s^* denote the amplitude ratios for the gas having the same viscosity as the water and an incident wave frequency of 10 Hz

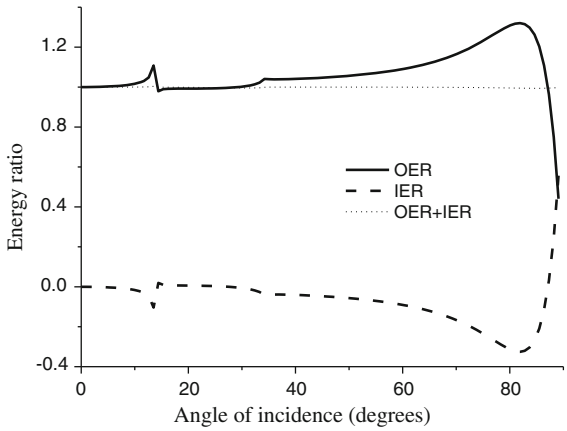

Figure 15
Orthodox energy flux and interference energy flux as a function of incidence angle for a plane SV wave of frequency 100 kHz in gas-saturated sand impinging on an interface with water-saturated sand. Note that the total energy flux (orthodox plus interference) is equal to 1

loss was observed to increase with increasing frequency as $\sqrt{f}$. The shapes of the reflection/transmission coefficient curves we find for incident SV at seismic frequencies (10–100 Hz) are much more complex than those of Dutta and Odé (1983) for incident P, which only exhibit single inflection points. A physical explanation of the observed numerical behavior is not obvious but is most likely related to the different coupling mechanisms between incident S and incident P. Very little mode conversion to the slow P wave occurs for an incident S wave.

The amplitude ratio curves (Fig. 13) and the energy ratio curves (Fig. 14) for the much higher (ultrasonic) frequency (100 kHz) case of an incident S wave show the almost non-existence of the Biot slow wave. Furthermore, the gas–water interface is non-reflective for incidence angles below 60°. The unusual definitive angle which occurs for the 10 Hz frequency disappears in Figs. 13 and 14. This gives a hint that this unusual definitive angle of 44° is related to fluid viscosity.

To verify such a supposition, we calculated the coefficients for the same interface at a frequency of 10 Hz, but changed the viscosity of the gas and water separately. Firstly, we changed the viscosity of the gas to be the same as that of the water (0.001 kg m^{-1} s^{-1}). In this case, the gas-filled sand has a transition frequency of 1,434 Hz. The incident wave frequency is then below the transition frequencies on both sides of the boundary. The amplitude ratios and energy ratios of the reflected and transmitted SV wave are denoted as R_s*, T_s*, REs* and TEs* respectively and are shown in Figs. 13 and 14. It is evident that they are very similar to the original R_s, T_s, REs and TEs curves. The interference energy fluxes are negligible at near-normal incidence and become negative with increasing angle, before rising sharply to equal the orthodox fluxes of +0.5 at an incidence angle of 90° (see Fig. 15).

Next, the viscosity of the water was set to be the same as that of the gas (1.0e−5 kg m^{-1} s^{-1}) and the transition frequency of the water-filled sand is changed to 2.2 Hz. In this case, the wave frequency (10 Hz) is greater than the transition frequency of the water-filled sand, but less than that of the gas-filled sand (21.5 Hz). Although the results are not shown here, we obtained similar curves to the original case of a 10 Hz wave as depicted in Figs. 11 and 12, and the unusual definitive angle appears again.

It is clear that the conditions for the unusual (diagnostic) angle to appear are that the incident wave frequency is below the transition frequency of the medium on at least one side of the boundary, so that the viscosity dominates the fluid property; the viscosities of the fluids on both sides of the boundary can be either the same or different. However, for the same viscosities,

the unusual angle appears when the transition frequency of one side is greater than the incident wave frequency. Therefore, the unusual angle at which the abrupt change in the curves occurs is caused by the change in viscosity of the pore fluid and provides a possible new means for recovering fluid properties from SV wave incidence in seismic surveying.

6. Conclusions

By applying Biot's poroelasticity theory, we have theoretically formulated the reflection and transmission coefficients for SV wave incidence at an interface between two different poroelastic solids. The coefficients are given in the forms of P and S wave amplitude ratios and energy ratios. They have been numerically calculated as a function of incidence angle and frequency for an interface between two different porous rocks and a gas–water interface in sand.

Plane SV wave incidence does not significantly excite the slow Biot P if the incident wave frequency is below the transition frequency. Above this frequency, plane SV waves can cause mode-converted Biot second (slow) P waves, which are actually normally propagative and not diffusive.

For an incident SV wave on a gas–water interface, there is a very different response than in the case of P wave incidence. For P wave incidence, the gas–water interface, like the interface separating two different porous rocks, will cause significant energy loss by mode conversion to the Biot slow P wave, especially as the frequency increases. But for SV wave incidence, there is no significant conversion to the Biot slow wave, even at very high incident wave frequency. For small incidence angles, the gas–water interface is almost transparent. However, with increasing angle of incidence, there is an unusual "definitive angle" in the reflection coefficient response which is related to the difference of fluid viscosity across the interface and it is a possible new means for underground fluid discrimination.

Acknowledgments

This research was supported by grants from the Australian Research Council and the Swiss National Science Foundation. One of us (XL) also wishes especially to acknowledge the University of Adelaide and the Faculty of Sciences for providing him with a postgraduate research scholarship during his doctoral studies. We very much appreciate the constructive comments of an anonymous reviewer and the editor, Dr. Arthur Snoke, which have improved the clarity of the manuscript.

Appendix A: Biot's Complex Wavenumbers, Dynamic Permeability and Constitutive Equations

The complex wavenumber for the Biot shear wave is given by:

$$k_s^2 = \frac{\omega^2}{\mu}\left(\rho - \frac{\rho_f^2}{q(\omega)}\right) \tag{47}$$

where ω is frequency; ρ_f and ρ is the density of the fluid and the average density of the composite; μ is the shear modulus of the solid frame; $q(\omega) = i\eta/\omega\kappa(\omega)$ and η is dynamic viscosity (or viscosity) and $\kappa(\omega)$ is the dynamic permeability (see later in this section).

The Biot slow P wave and the classic P wave have wavenumbers:

$$k_d^2 = \omega^2 \frac{c_1\delta_{22} - c_3\delta_{12}}{c_1c_4 - c_2c_3} \tag{48}$$

$$k_c^2 = \omega^2 \frac{c_2\delta_{21} - c_4\delta_{12}}{c_3c_2 - c_1c_4} \tag{49}$$

where

$$\left.\begin{array}{ll} \delta_{11} = \rho\delta_d + \rho_f & c_1 = (\lambda_c + 2\mu)\delta_d + \alpha M \\ \delta_{12} = \rho\delta_c + \rho_f & c_2 = (\lambda_c + 2\mu)\delta_c + \alpha M \\ \delta_{21} = \rho_f\delta_d + q(\omega) & c_3 = \alpha M\delta_d + M \\ \delta_{22} = \rho_f\delta_c + q(\omega) & c_4 = \alpha M\delta_c + M \end{array}\right\} \tag{50}$$

$$\delta_c = \frac{-B - \sqrt{B^2 - 4AC}}{2A} \quad \text{and}$$
$$\delta_d = \frac{-B + \sqrt{B^2 - 4AC}}{2A} \tag{51}$$

$$\left.\begin{array}{r} A = \rho\alpha M - \rho_f(\lambda_c + 2\mu) \\ B = \rho M - q(\omega)(\lambda_c + 2\mu) \\ C = -q(\omega)\alpha M + M\rho_f \end{array}\right\} \tag{52}$$

$$\lambda_c = K_m - 2\mu/3 + \alpha^2 M \tag{54}$$

$$\alpha = 1 - \frac{K_m}{K_s} \tag{55}$$

$$\frac{1}{M} = \frac{\alpha}{K_s} + n\left(\frac{1}{K_f} - \frac{1}{K_s}\right) \tag{56}$$

Here, K_s, K_f and K_m are the bulk modulus of the solid grain, the pore fluid and the solid frame, respectively.

The dynamic permeability can be viewed as static permeability κ_0 multiplied by a frequency correction factor (Johnson *et al.* 1978),

$$\kappa(\omega) = \kappa_0\left[\sqrt{1 - i\frac{4\omega}{n_J\omega_t}} - i\frac{\omega}{\omega_t}\right]^{-1} \tag{57}$$

$$\omega_t = \eta/(\rho_f F \kappa_0) \tag{58}$$

Here, κ_0 is permeability; ω_t is called the transition frequency or relaxation frequency (Pride *et al.* 2004) which separates the viscous force-dominated flow from the inertial force-dominated flow. The quantity $n_J = \Lambda^2/\kappa_0 F$, where Λ represents the pore volume-to-surface ratio and has the dimensions of length. F is the electric formation factor and it can also be related to the tortuosity T and porosity n through the relation: $F = Tn^{-1}$.

Biot's constitutive equations can be written as

$$\tau_{ij} = 2\mu e_{ij} + \delta_{ij}(\lambda_c e - \alpha M\zeta) \tag{59}$$

$$p_f = -\alpha M e + M\zeta \tag{60}$$

Here, τ_{ij} = total stress in the medium (including the porous solid frame and the fluid filling the pores); p_f = fluid pressure in the pores; e = div $\mathbf{u}$; $\zeta = -$div $\mathbf{w}$;

$$e_{ij} = \frac{1}{2}\left(\frac{\partial u_i}{\partial x_j} + \frac{\partial u_j}{\partial x_i}\right), \tag{61}$$

and

δ_{ij} is the Kronecker delta symbol.

Appendix B: The Reflection and Transmission Coefficients for an Incident SH Wave

Because SH waves are decoupled from P-SV waves in isotropic media, and incident SH waves do not mode-convert to P or to SV waves, the boundary conditions, Eqs. 8 and 9a, which are just related to the compressional properties, are not required. So there will only be three waves to consider: incident SH, reflected SH and transmitted SH.

The relative fluid displacement for the incident SH shear wave $\mathbf{w}_{sh}$, is written as:

$$\mathbf{w}_{sh} = A_{sh}\exp(il_{1s}y)\exp(im_{1s}x - i\omega t)\hat{\mathbf{z}} \tag{61}$$

Let $\mathbf{w}_{1s}$ be the reflected wave in medium 1, given by:

$$\mathbf{w}_{1s} = B_{1s}\exp(-il_{1s}y)\exp(im_{1s}x - i\omega t)\hat{\mathbf{z}} \tag{62}$$

Let $\mathbf{w}_{2s}$ be the transmitted waves in medium 2, given by:

$$\mathbf{w}_{2s} = A_{2s}\exp(il_{2s}y)\exp(im_{2s}x - i\omega t)\hat{\mathbf{z}} \tag{63}$$

where l_{js} and m_{js}, (j = 1, 2) denote, respectively, the x- and y-components of the complex wave vector k_{js} of medium j (The waves propagate in the x–y plane). The total wavenumber is given by:

$$(l_{js})^2 + (m_{js})^2 = (k_{js})^2 \tag{64}$$

From the continuity condition of the solid frame displacement, Eq. (6) and the linear relationship, Eq. (4), which are valid for all x and t, we have:

$$m_{1s} = m_{1s} \tag{65}$$

$$\Gamma_{1s}(A_{sh} + B_{1s}) = \Gamma_{2s}(A_{2s}) \tag{66}$$

By the continuity condition of the total traction, Eq. 7, we have:

$$\mu_1 l_{1s}\Gamma_{1s}(A_{sh} - B_{1s}) = \mu_2 l_{2s}\Gamma_{2s}A_{2s} \tag{67}$$

By Eqs. 66 and 67, we get the transmission ratio of the relative fluid displacement A_{2s}/A_{sh},

$$\frac{A_2}{A_{sh}} = \frac{2\mu_1 l_{1s}\Gamma_{1s}}{(\mu_1 l_{1s} + \mu_2 l_{2s})\Gamma_{2s}} \tag{68}$$

and the reflection ratio of the relative fluid displacement B_{1s}/A_{sh},

$$\frac{B_{1s}}{A_{sh}} = \frac{(\mu_1 l_{1s} - \mu_2 l_{2s})}{(\mu_1 l_{1s} + \mu_2 l_{2s})} \tag{69}$$

According to Eq. 69, if the physical parameters of the two media are the same, the reflection goes to zero. Then, by Eq. 4, the transmission coefficient of the solid frame displacement is:

$$T_{\mathrm{sh}} = \frac{A_{2\mathrm{s}}\Gamma_{2\mathrm{s}}}{A_{\mathrm{sh}}\Gamma_{1\mathrm{s}}} \tag{70}$$

The reflection coefficient of the solid frame displacement is:

$$R_{\mathrm{sh}} = \frac{B_{1\mathrm{s}}}{A_{\mathrm{sh}}} \tag{71}$$

Appendix C: The Coefficients of the Boundary Conditions

The elements a_{ij} of matrix A appearing in Eq. 31 are obtained as follows:

(i) Setting $u_{1x} = u_{2x}$

$$a_{11} = 1, \quad a_{12} = -\frac{\Gamma_{1\mathrm{c}} m}{\Gamma_{1\mathrm{s}} l_{1\mathrm{s}}}, \quad a_{13} = -\frac{\Gamma_{1\mathrm{d}} m}{\Gamma_{1\mathrm{s}} l_{1\mathrm{s}}},$$
$$a_{14} = \frac{\Gamma_{2\mathrm{s}} l_{2\mathrm{s}}}{\Gamma_{1\mathrm{s}} l_{1\mathrm{s}}}, \quad a_{15} = \frac{\Gamma_{2\mathrm{c}} m}{\Gamma_{1\mathrm{s}} l_{1\mathrm{s}}}, \quad a_{16} = \frac{\Gamma_{2\mathrm{d}} m}{\Gamma_{1\mathrm{s}} l_{1\mathrm{s}}}$$

(ii) Setting $u_{1y} = u_{2y}$

$$a_{21} = -1, \quad a_{22} = -\frac{\Gamma_{1\mathrm{c}} l_{1\mathrm{c}}}{\Gamma_{1\mathrm{s}} m}, \quad a_{23} = -\frac{\Gamma_{1\mathrm{d}} l_{1\mathrm{d}}}{\Gamma_{1\mathrm{s}} m},$$
$$a_{24} = \frac{\Gamma_{2\mathrm{s}}}{\Gamma_{1\mathrm{s}}}, \quad a_{25} = -\frac{\Gamma_{2\mathrm{c}} l_{2\mathrm{c}}}{\Gamma_{1\mathrm{s}} m}, \quad a_{26} = -\frac{\Gamma_{2\mathrm{d}} l_{2\mathrm{d}}}{\Gamma_{1\mathrm{s}} m}$$

(iii) Setting $\tau_{1yy} = \tau_{2yy}$

$$a_{31} = 1, \quad a_{34} = \frac{\mu_2 \Gamma_{2\mathrm{s}} l_{2\mathrm{s}}}{\mu_1 \Gamma_{1\mathrm{s}} l_{1\mathrm{s}}},$$
$$a_{32} = \frac{[\Gamma_{1\mathrm{c}}(\lambda_{1\mathrm{c}} + 2\mu_1) + \alpha_1 M_1](k_{1\mathrm{c}})^2 - \Gamma_{1\mathrm{c}} 2\mu_1 m^2}{\Gamma_{1\mathrm{s}} 2\mu_1 m l_{1\mathrm{s}}},$$
$$a_{33} = \frac{[\Gamma_{1\mathrm{d}}(\lambda_{1\mathrm{c}} + 2\mu_1) + \alpha_1 M_1](k_{1\mathrm{d}})^2 - \Gamma_{1\mathrm{d}} 2\mu_1 m^2}{\Gamma_{1\mathrm{s}} 2\mu_1 m l_{1\mathrm{s}}},$$
$$a_{35} = \frac{\Gamma_{2\mathrm{c}} 2\mu_2 m^2 - [\Gamma_{2\mathrm{c}}(\lambda_{2\mathrm{c}} + 2\mu_2) + \alpha_2 M_2](k_{2\mathrm{c}})^2}{\Gamma_{1\mathrm{s}} 2\mu_1 m l_{1\mathrm{s}}},$$
$$a_{36} = \frac{\Gamma_{2\mathrm{d}} 2\mu_2 m^2 - [\Gamma_{2\mathrm{d}}(\lambda_{2\mathrm{c}} + 2\mu_2) + \alpha_2 M_2](k_{2\mathrm{d}})^2}{\Gamma_{1\mathrm{s}} 2\mu_1 m l_{1\mathrm{s}}}$$

(iv) Setting $\tau_{1xy} = \tau_{2xy}$

$$a_{41} = -1, \quad a_{42} = \frac{\Gamma_{1\mathrm{c}} 2 m l_{1\mathrm{c}}}{\Gamma_{1\mathrm{s}}(l_{1\mathrm{s}}^2 - m^2)}, \quad a_{43} = \frac{\Gamma_{1\mathrm{d}} 2 m l_{1\mathrm{d}}}{\Gamma_{1\mathrm{s}}(l_{1\mathrm{s}}^2 - m^2)},$$
$$a_{44} = \frac{\Gamma_{2\mathrm{s}}\mu_2(l_{2\mathrm{s}}^2 - m^2)}{\Gamma_{1\mathrm{s}}\mu_1(l_{1\mathrm{s}}^2 - m^2)}, \quad a_{45} = \frac{\Gamma_{2\mathrm{c}} 2\mu_2 m l_{2\mathrm{c}}}{\Gamma_{1\mathrm{s}}\mu_1(l_{1\mathrm{s}}^2 - m^2)},$$
$$a_{46} = \frac{\Gamma_{2\mathrm{d}} 2\mu_2 m l_{2\mathrm{d}}}{\Gamma_{1\mathrm{s}}\mu_1(l_{1\mathrm{s}}^2 - m^2)}$$

(v) Setting $w_{1y} = w_{2y}$

$$a_{51} = -1, \quad a_{52} = -\frac{l_{1\mathrm{c}}}{m}, \quad a_{53} = -\frac{l_{1\mathrm{d}}}{m},$$
$$a_{54} = 1, \quad a_{55} = -\frac{l_{2\mathrm{c}}}{m}, \quad a_{56} = -\frac{l_{2\mathrm{d}}}{m},$$

(vi) Setting $\frac{\partial}{\partial t} w_{2y} = \kappa_{12}(p_{1f} - p_{2f})$

$$a_{61} = 0, \quad a_{62} = \kappa_{12}(\alpha_1 \Gamma_{1\mathrm{c}} + 1) M_1 (k_{1\mathrm{c}})^2$$
$$a_{63} = \kappa_{12}(\alpha_1 \Gamma_{1\mathrm{d}} + 1) M_1 (k_{1\mathrm{d}})^2, \quad a_{64} = \omega m$$
$$a_{65} = -(\omega l_{2\mathrm{c}} + \kappa_{12}(\alpha_2 \Gamma_{2\mathrm{c}} + 1) M_2 k_{2\mathrm{c}}^2)$$
$$a_{66} = -(\omega l_{2\mathrm{d}} + \kappa_{12}(\alpha_2 \Gamma_{2\mathrm{d}} + 1) M_2 k_{2\mathrm{d}}^2)$$

For the sealed-pore boundary condition, $\kappa_{12} = 0$, then

$$a_{61} = a_{62} = a_{63} = 0, \quad a_{64} = \omega m,$$
$$a_{65} = -\omega l_{2\mathrm{c}}, \quad a_{66} = -\omega l_{2\mathrm{d}}$$

For the open-pore boundary condition, $\kappa_{12} = \infty$, then

$$a_{61} = a_{64} = 0,$$
$$a_{62} = (\alpha_1 \Gamma_{1\mathrm{c}} + 1) M_1 k_{1\mathrm{c}}^2, \quad a_{63} = (\alpha_1 \Gamma_{1\mathrm{d}} + 1) M_1 k_{1\mathrm{d}}^2,$$
$$a_{65} = -(\alpha_2 \Gamma_{2\mathrm{c}} + 1) M_2 k_{2\mathrm{c}}^2, \quad a_{66} = -(\alpha_2 \Gamma_{2\mathrm{d}} + 1) M_2 k_{2\mathrm{d}}^2$$

References

Aki, K. and Richards, P.G. (1980). Quantitative Seismology: Theory and Methods-Vols. *I–II*, W.H. Freeman, San Francisco.

Biot, M.A. (1956a). *Theory of propagation of elastic waves in a fluid-saturated porous solid: I- low frequency range*. Journal of the Acoustical Society of America, *28*(2):168–178.

Biot, M.A. (1956b). *Theory of propagation of elastic waves in a fluid-saturated porous solid: II-higher frequency range*. Journal of the Acoustical Society of America, *28*(2):179–191.

Denneman, A.I.M., Drijkoningen, G.G., Smeulders, D.M. and Wapenaar, K. (2002). *Reflection and transmission of waves at a fluid/porous-medium interface.* Geophysics *67*:282–291.

Deresiewicz, H. and Skalak, R. (1963). *On uniqueness in dynamic poroelasticity*. Bulletin of Seismological Society of America, *53*:783–788.

Dutta, N.C. and Odé, H. (1979a). *Attenuation and dispersion of compressional waves in fluid-filled porous rocks with partial gas saturation (White model)-Part I: Biot theory*. Geophysics, *44*(11):1777–1788.

Dutta, N.C. and Odé, H. (1979b). *Attenuation and dispersion of compressional waves in fluid-filled porous rocks with partial gas saturation (White model)-Part II: Results*. Geophysics, *44*(11):1789–1805.

DUTTA, N.C. and ODÉ H. (1983). *Seismic reflections from a gas-water contact*. Geophysics *48*(2):148–162.

GASSMANN, F. (1951). Über die elastizität poröser medien: Viertel. Nat rurforsch. Ges., Zurich *96*:1–23.

GEERTSMA, J. and SMIT, D.C. (1961). *Some aspects of elastic wave propagation in fluid-saturated porous solids*. Geophysics, *26*(2):169–181.

GUREVICH, B. and SCHOENBERG, M. (1999). *Interface conditions for Biot's equations of poroelasticity.* Journal of the Acoustical Society of America, *105*:2285–2589.

GUREVICH, B., CIZ, R: and DENNEMAN, A.I.M. (2004). *Simple expressions for normal incidence reflection coefficients from an interface between fluid-saturated porous materials.* Geophysics *69*:1372–1377.

JOHNSON, D. L., KOPLIK, J. and DASHEN, R. (1978). *Theory of dynamic permeability and tortuosity in fluid-saturated porous media.* Journal of Fluid Mechanics, *176*:379–402.

PRIDE, S.R., BERRYMAN, J.G. and HARRIS, J.M. (2004). *Seismic attenuation due to wave-induced flow*. Journal of Geophysical Research, *109*:B01201:1–19.

QUIROGA-GOODE, G. and CARCIONE, J.M. (1997). *Heterogeneous modelling behaviour at an interface in porous media*. Computational Geosciences, *1*:109–125.

SANTOS, J.E., CORBERO, J.M., RAVAZOLLI, C.L. and HENSLEY, J.L. (1992). *Reflection and transmission coefficients in fluid-saturated porous media*. Journal of the Acoustical Society of America, *91*(4):1911–1923.

SHARMA, M.D., KAUSHIK, V.P. and GOGNA, M.L. (1990). *Reflection and refraction of plane waves at an interface between liquid-saturated porous solid and viscoelastic solid*. The Quarterly Journal of Mechanics and Applied Mathematics, *43*(4):427–448.

SHARMA, M.D. and SAINI, T. (1992). *Pore alignment between two dissimilar saturated poroelastic media: Reflection and refraction at the interface*. Int. J. Solids Structures, *29*(11):1361–1377.

SHARMA, M.D. (2008). *Wave propagation across the boundary between two dissimilar poroelastic solids*. Journal of Sound and Vibration, *314*:657–671.

WU, K.Y., XUE, Q. and ADLER, L. (1990). *Reflection and transmission of elastic waves from a fluid-saturated porous solid boundary*. Journal of the Acoustical Society of America, *87*(6):2349–2358.

YANG, J. (1999). *Importance of flow condition on seismic waves at saturated porous solid boundary*. Journal of Sound and Vibration, *221*(3):391–413.

(Received November 29, 2013, revised March 25, 2014, accepted March 26, 2014, Published online April 11, 2014)